RESEARCH PAPER

Structure-Based Identification Of Telomerase Inhibitors From Andrographis Paniculata

Quan Ke Thai[1*], Phuoc Huynh[2], Ba-Hai Nguyen[3], Phuong Nguyen Ngoc[4]

[1]Faculty of Natural Science Education, Saigon University, 273 An Duong Vuong, Cho Quan Ward, Ho Chi Minh City, Vietnam, 700000
Email: tkquan@sgu.edu.vn
ORCID: 0000-0002-2264-2579

[2]Graduate University of Science and Technology, Vietnam Academy of Science and Technology, Vietnam
Email: phuoc.huynh140299@gmail.com
ORCID: 0000-0003-3066-4580

[3]Faculty of Pharmacy, Binh Duong Medical College, 529 Le Hong Phong, Phu Loi Ward, Ho Chi Minh City, Vietnam

[4]Ho Chi Minh City University of Education, 280 An Duong Vuong Street, Cho Quan Ward, Ho Chi Minh City, Vietnam, Email: phuongnn@hcmue.edu.vn, ORCID: 0009-0009-7189-8843

Corresponding author: Quan Ke Thai
Email: tkquan@sgu.edu.vn

ABSTRACT

Elevated telomerase expression is a hallmark of many human malignancies. Targeting telomerase represents a promising therapeutic strategy, as it is largely absent in normal cells. However, the limitations and side effects of synthetic chemical inhibitors remain a challenge for sustained treatment. Consequently, the exploration of alternative remedies derived from medicinal plants, particularly as combination therapies, may help minimize adverse effects. *Andrographis paniculata* (AP) has long been employed in traditional medicine for cancer treatment. Among its constituents, Andrographolide is recognized as the principal compound underlying its anticancer activity. Nevertheless, the mechanism by which Andrographolide and its derivatives modulate telomerase activity has not been clearly elucidated. In this study, we screened Andrographolide and its derivatives from AP for their ability to bind the telomerase pocket using molecular docking and molecular dynamics simulations. Simulation results over 200 ns revealed that Andrographolide and two derivatives, LTS0109188 and LTS0004521, established stable and effective interactions with telomerase. Binding affinity evaluation through free energy analyses indicated that these compounds exhibited stronger affinity than the reference inhibitor BIBR1532. Accordingly, we report that Andrographolide, LTS0109188, and LTS0004521 may inhibit telomerase activity in a manner comparable to BIBR1532. Furthermore, pharmacological profiling demonstrated that these compounds fulfill most drug-likeness criteria, supporting their suitability for oral drug development. Toxicity assessment and anticancer bioactivity prediction further highlighted the potential of Andrographolide, LTS0109188, and LTS0004521 as promising candidates for cancer therapy.

Keywords: *Andrographis paniculata,* Andrographolide, cancer, molecular docking, dynamic simulations, telomerase.

How to cite this article: Thai QK, Huynh P, Nguyen BH, Ngoc PN. Structure-Based Identification Of Telomerase Inhibitors From Andrographis Paniculata. Int J Drug Deliv Technol. 2026;16(6s): 725-736; DOI: 10.25258/ijddt.16.6s.99

Source of support: Nil.

Conflict of interest: None

INTRODUCTION

Cancer remains a leading cause of mortality worldwide, accounting for millions of deaths annually, as reported by GLOBOCAN[1]. Among the most prevalent malignancies are lung cancer, breast cancer in women, colorectal cancer, prostate cancer, and gastric cancer[1]. The immortality of cancer cells is largely attributed to telomerase activation, which stabilizes and elongates chromosomal telomeres[2]. Numerous studies have demonstrated a close association between aberrant telomerase activity and a wide range of cancers, including breast, renal, colorectal, cervical, lung, hepatic, pancreatic, thyroid, prostate, and bladder cancers[3,4,5]. Indeed, excessive telomerase expression is implicated in approximately 90% of human malignancies[6,7]. Thus establishing telomerase as an ideal therapeutic target for broad-spectrum cancer treatment[8,9]. Importantly, while

telomerase is minimally expressed in most normal cells, it serves as a hallmark of tumor cells[10]. This differential expression underscores the potential for telomerase-targeted therapies to selectively affect cancer cells while reducing side effects relative to conventional chemotherapy and radiotherapy.

Telomerase is a ribonucleoprotein composed of two essential components: the telomerase reverse transcriptase (TERT) and the telomerase RNA component (TERC) [2,11]. TERT functions as a reverse transcriptase responsible for elongating chromosomal ends and maintaining genome integrity[12], whereas TERC provides the RNA template for telomeric repeat addition during terminal extension[2]. Strategies to inhibit telomerase have shown that strong inhibition of TERT can trigger progressive telomere shortening, ultimately leading to cancer cell death[13]. Consequently, multiple approaches, including the use of small molecules, have been employed to inhibit telomerase activity through direct interaction with TERT[14]. Among these, the small-molecule inhibitor BIBR1532 was specifically developed to target TERT activity[15]. Extensive studies have demonstrated its tumor-suppressive potential, making it a promising candidate for cancer therapy[16,17,18]. In addition to synthetic inhibitors, naturally derived plant compounds have emerged as a promising avenue in cancer treatment[19]. Many natural products are incorporated into diets, offering high safety profiles and broad acceptance in cancer management[20]. Beyond telomerase inhibition via TERT, natural compounds can also induce apoptosis, activate p53 expression, and suppress tumor growth and metastasis[21,22,23]. Given the vast diversity of medicinal plants, the search for bioactive compounds with telomerase-inhibitory potential remains a critical endeavor in the development of novel anticancer therapies.

Andrographis paniculata (Burm. f.) Wall. ex Nees, a member of the Acanthaceae family, has attracted increasing attention over the past decade for its diverse secondary metabolites[24]. Native to India and Sri Lanka, the plant is widely distributed across Southeast Asian countries, including Vietnam, China, Indonesia, Thailand, Malaysia, Myanmar, and the Philippines[25,26,27]. *A. paniculata* (AP) is one of the most important and extensively used herbs in traditional medicine[28]. Almost all parts of the plant are employed in folk remedies across Asia and Europe[27,29]. The pharmacological potential of AP, particularly its anticancer activity, has been intensively investigated[30,31,32,33]. Phytochemical studies have identified numerous constituents of AP[34,35] with Andrographolide recognized as its principal bioactive compound[36,37]. Owing to its unique biological activities, Andrographolide has been commercialized in various products, and its purified form holds significant economic value, estimated at approximately USD 100,000 per kilogram[38]. Extensive studies have demonstrated that Andrographolide suppresses multiple cancer types by modulating diverse signaling pathways[39,40,41]. Recent reports have suggested that Andrographolide may inhibit telomerase activity[42,43]. However, the molecular mechanism underlying this inhibition remains insufficiently characterized[44]. Here, we provide mechanistic insights into the telomerase-inhibitory potential of Andrographolide and its derivatives, revealed through molecular dynamics simulations. Our findings establish a molecular framework that links this widely used medicinal compound to telomerase inhibition, highlighting its promise as a natural scaffold for anticancer drug development.

MATERIALS AND METHODS

Molecular docking system construction with telomerase

Natural compounds from *A. paniculata* (AP) were retrieved from the LOTUS database, as described in our previous study[21]. The structures of these compounds were optimized and converted into appropriate formats using OpenBabel[45] for virtual screening.

The crystal structure of telomerase in complex with BIBR1532 (PDB ID: 5CQG) was obtained from the Protein Data Bank and used as a reference model for docking simulations[15]. The telomerase protein structure was prepared and optimized using Maestro (Academic version). Docking input files were generated with AutoDock Tools[46], where the BIBR1532-binding site was defined as the docking pocket for AP compounds. A grid box of 50 × 50 × 50 Å with a spacing of 0.375 Å was centered at coordinates x = 1.768, y = –1.392, and z = 11.868. Docking simulations were performed using AutoDock GPU[47], with 1000 iterations for each compound. Protein–ligand interactions were analyzed using the Protein–Ligand Interaction Profiler (PLIP) server[48].

Physicochemical properties, pharmacokinetics, toxicity, and anticancer activity

Physicochemical and pharmacokinetic properties were evaluated using the SwissADME server[49], while toxicity profiles were predicted using pkCSM[50] . Compounds that satisfied drug-likeness criteria (Lipinski's rule of five) and exhibited non-toxic profiles were subjected to further analysis. Their anticancer-related bioactivities were predicted using

the PASS server[51], with a probability of activity (P_a) ≥ 0.3 considered indicative of anticancer potential.

Molecular dynamic simulations

Molecular dynamics simulations (MDS) were employed to evaluate the stability of compounds within the telomerase binding pocket. Ligand topology files were generated using the SwissParam server[52] based on the CHARMM force field. The simulation systems were constructed and executed in GROMACS[53]. using the CHARMM36 force field[54] , with recommended interaction parameters. Specifically, the LINCS algorithm was applied for bond constraints; a Coulomb cutoff of 1.2 nm was used; short-range van der Waals interactions were truncated at 1.2 nm; and long-range electrostatics were treated with the Particle Mesh Ewald (PME) method. Protein–ligand complexes were solvated in a cubic box with a minimum distance of 1.0 nm from the box edge, filled with TIP3P water molecules, and neutralized with 0.15 M NaCl. Energy minimization was performed until the system reached its lowest-energy state. Equilibration was carried out in two phases: NVT and NPT ensembles, each for 100 ps, using a V-rescale thermostat at 300 K and a C-rescale barostat at 1 atm. Production simulations were performed for 200 ns with a time step of 2 fs, and trajectories were recorded every 10 ps. Post-simulation analyses included root mean square deviation (RMSD)**,** radius of gyration (Rg)**,** and number of protein–ligand contacts, calculated using the built-in *rms*, *gyrate*, and *mindist* functions in GROMACS. Residue-level interactions between telomerase and ligands in MDS were further examined using an in-house Python script based on PLIP.

Binding free energy analysis

The binding affinity of compounds to telomerase during MDS was quantified using binding free energy calculations. These values were estimated via the MM/GBSA approach, widely applied to protein–ligand systems[55,56,57]. In this study, the gmx_MMPBSA tool[58] was employed to compute binding free energy from GROMACS trajectories according to Equation (1):

$$\Delta G_{MM/GBSA} = \Delta G_{Complex} - \Delta G_{Protein} - \Delta G_{ligand} \quad (1)$$

Each free energy component was estimated as shown in Equation (2):

$$\Delta G = \Delta G_{vdW} + \Delta G_{Eletrostatic} + \Delta G_{GB} + \Delta G_{Non-polar} \quad (2)$$

here, $G_{Eletrostatic}$, and ΔG_{vdW} represent the van der Waals and electrostatic interaction energies between the protein and ligand, respectively, while ΔG_{GB} and $\Delta G_{Non-polar}$ denote the polar and non-polar contributions to solvation free energy.

RESULTS

Molecular screening

The docking protocol was first validated by re-docking the reference inhibitor BIBR1532 into the telomerase binding pocket (Figure 1). The root-mean-square deviation (RMSD) between the re-docked pose and its crystallographic conformation was 0.71 Å, with a binding affinity of –10.02 kcal/mol, confirming the reliability of the docking setup. Subsequent virtual screening of AP compounds identified Andrographolide (LTS0072631) and two derivatives, LTS0109188 and LTS0004521, as strong binders to the telomerase pocket, showing binding modes comparable to BIBR1532 (Figure 1). Binding energy analysis revealed that LTS0109188 (–11.74 kcal/mol), LTS0004521 (–11.72 kcal/mol), and Andrographolide (–11.60 kcal/mol) all exhibited stronger affinities toward telomerase than BIBR1532 (–10.02 kcal/mol) (Table 1). Phyto-origin tracing confirmed that all three compounds belong to the diterpenoid class and are characteristic constituents of *A. paniculata*, as annotated in the LOTUS database (Table 2).

Table 1: Chemical structures of Andrographolide and its derivatives bound to telomerase.

LOTUS ID	Common name	Molecular structure	Binding free energy
LTS0109188	-	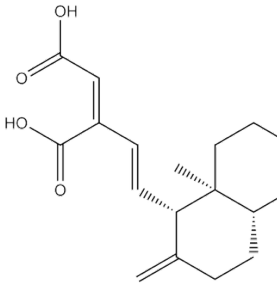	-11.74
LTS0004521	-	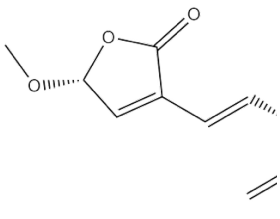	-11.72
LTS0072631	Andrographolide	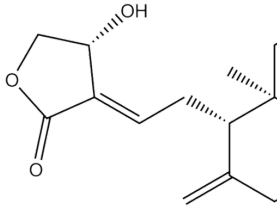	-11.60

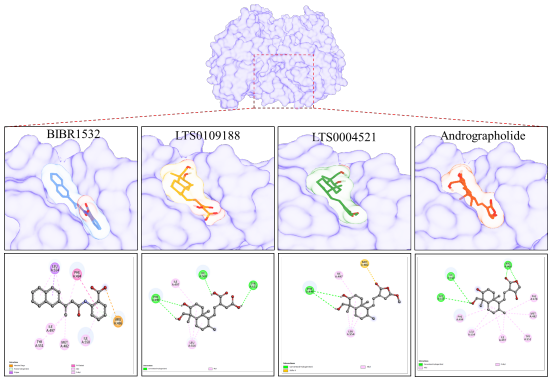

Figure 1: Binding poses of *A. paniculata* compounds within the telomerase pocket. *(The figure illustrates binding positions and key interactions for BIBR1532, LTS0109188, LTS0004521, and Andrographolide.)*

Table 2: Chemical class and biological origin of Andrographolide and its derivatives, as annotated in the LOTUS database.

LOTUS ID	Wikidata ID	Chemical superclass	Class	Organism source
LTS0109188	Q105115613	Diterpenoids	Labdane diterpenoids	*Andrographis paniculata*
LTS0004521	Q104966409	Diterpenoids	Labdane diterpenoids	*Andrographis paniculata*
LTS0072631	Q104939270	Diterpenoids	Labdane diterpenoids	*Andrographis paniculata*

Physiochemical and pharmacokinetics profiling

We next evaluated the pharmacological and toxicity properties of Andrographolide and its two derivatives. Pharmacokinetic predictions using SwissADME are summarized in Table 3. All three compounds strictly complied with major drug-likeness criteria, including Lipinski's rule of five, Ghose, Veber, Egan, and Muegge filters. They were predicted to be water-soluble with high gastrointestinal absorption (Table 3), suggesting that Andrographolide and its derivatives are suitable for oral administration. To further assess safety, potential toxicities were examined using the pkCSM web server. Predictions indicated that the compounds are non-mutagenic (negative AMES test), do not inhibit cardiac hERG I or hERG II receptors, and are neither hepatotoxic nor skin irritants (Table 4). Collectively, these findings support a favorable safety profile. Based on pharmacokinetic (Table 3) and toxicity assessments (Table 4), Andrographolide and its derivatives emerge as promising candidates for future drug development.

Table 3: Molecular properties and pharmacological profiles of the investigated compounds.

	LTS0109188	LTS0004521	Andrographolide
Formula	C20H28O6	C21H30O5	C20H30O5
Molecular weight	364.43 g/mol	362.46 g/mol	350.45 g/mol
Number of heavy atoms	26	26	25
Number of aromatic heavy atoms	0	0	0
Number of rotatable bonds	5	4	3
Number of H-bond acceptor	6	5	5
Number of H-bond donor	4	2	3
TPSA	115.06 Å²	75.99 Å²	86.99 Å²
Water Solubility	Soluble	Soluble	Soluble
GI absorption	High	High	High
Lipinski rule	Yes	Yes	Yes
Ghose	Yes	Yes	Yes
Veber	Yes	Yes	Yes
Egan	Yes	Yes	Yes
Muegge	Yes	Yes	Yes

Table 4: Predicted toxicity profiles of the compounds obtained using the pkCSM server.

Properties	LTS0109188	LTS0004521	Andrographolide
AMES toxicity	No	No	No
hERG I inhibitor	No	No	No
hERG II inhibitor	No	No	No
Hepatotoxicity	No	No	No
Skin Sensitisation	No	No	No

Importantly, we explored their potential anticancer activities. PASS predictions indicated that all three compounds exhibited high probability (Pa) values for antineoplastic, anticarcinogenic, apoptosis agonist, anti-inflammatory, Myc inhibitor, and TP53 expression enhancer activities—properties highly relevant to multi-cancer inhibition. Notably, antineoplastic potential was predicted across multiple cancers, including breast, lung, and melanoma. Compound-specific associations were also observed: LTS0109188 with cervical cancer, Andrographolide with ovarian cancer, and both LTS0109188 and LTS0004521 with brain cancer. Colorectal and colon cancers were linked to a combined effect of LTS0004521 and Andrographolide. These results suggest that, beyond their broad antitumor potential, individual compounds may exert cancer-type–specific activities. Thus, combinatorial application of these diterpenoids could be particularly advantageous for cancer therapy.

Table 5: Predicted anticancer activities of the compounds based on the PASS server.

Properties	LTS0109188	LTS0004521	Andrographolide
	P_a		
Antineoplastic	0,897	0,891	0,949
Antineoplastic (breast cancer)	0,405	0,570	0,416
Antineoplastic (brain cancer)	0,403	0,335	-
Antineoplastic (lung cancer)	0,582	0,623	0,772
Antineoplastic (colorectal cancer)	-	0,362	0,547
Antineoplastic (colon cancer)	-	0,350	0,538
Antineoplastic (cervical cancer)	0,298	-	-
Antineoplastic (melanoma)	0,504	0,503	0,648
Antineoplastic (ovarian cancer)	-	-	0,333
Anticarcinogenic	0,570	0,337	0,475
Apoptosis agonist	0,860	0,299	0,909
Antiinflammatory	0,765	0,798	0,845
Myc inhibitor	0,555	0,465	0,471
TP53 expression enhancer	0,628	0,436	0,520

Molecular dynamics simulations (MDS)

Telomerase conformational dynamics in MDS

To further investigate binding stability, 200-ns molecular dynamics simulations (MDS) were performed for each compound in complex with telomerase. The root mean square deviation (RMSD) of the C_α backbone was used to evaluate conformational fluctuations. Low and stable RMSD values generally indicate tight ligand binding and strong affinity[59]. As shown in Figure 2A–D, telomerase bound to the reference inhibitor BIBR1532 displayed broad fluctuations across the 200-ns trajectory, with a dispersed RMSD distribution and a mean of 0.425 ± 0.068 nm (Figure 2A). In contrast, complexes with the AP compounds (LTS0109188, LTS0004521, and Andrographolide) were markedly more stable (Figure 2B–D). Among these, LTS0109188 and LTS0004521

showed the greatest stability, with tightly clustered RMSD distributions and means of 0.289 ± 0.041 nm and 0.273 ± 0.045 nm, respectively (Figure 2E). The telomerase–Andrographolide complex exhibited higher fluctuation toward the end of the simulation but maintained a lower average RMSD (0.337 ± 0.067 nm) than BIBR1532 (Figure 2E).

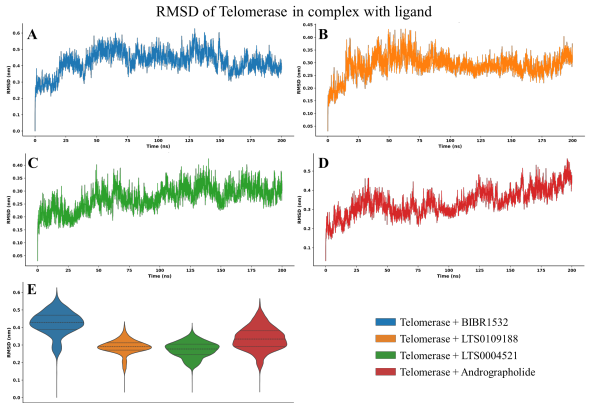

Figure 2: Root-mean-square deviation (RMSD) of telomerase during 200 ns MDS.

*((**A**) Telomerase + BIBR1532 (blue). **(B)** Telomerase + LTS0109188 (orange). **(C)** Telomerase + LTS0004521 (green). **(D)** Telomerase + Andrographolide (red). **(E)** Distribution of RMSD values across systems represented as violin plots.)*

We next assessed the influence of ligand binding on overall protein compactness using the radius of gyration (Rg). This parameter reflects the root mean square distance of protein atoms from the center of mass and provides insight into folding stability during MDS [60]. Lower Rg values typically correspond to more compact, stable protein conformations and potentially stronger ligand interactions[61,62]. Rg distributions over 200 ns are shown in Figure 3A–D. For the reference system, telomerase+BIBR1532 exhibited fluctuations with a mean Rg of 2.972 ± 0.026 nm. In comparison, the AP compounds promoted more compact conformations, with average Rg values of 2.923 ± 0.032 nm (LTS0109188), 2.920 ± 0.030 nm (LTS0004521), and 2.961 ± 0.034 nm (Andrographolide) (Figure 3E). Notably, the telomerase–LTS0004521 complex displayed the most stable Rg profile (Figure 3C), while LTS0109188 and Andrographolide showed higher fluctuations and a tendency toward expansion during the final 50 ns (Figure 3B,D). These results indicate that Andrographolide and its derivatives significantly modulate telomerase conformational dynamics, with LTS0004521 in particular enhancing structural stability.

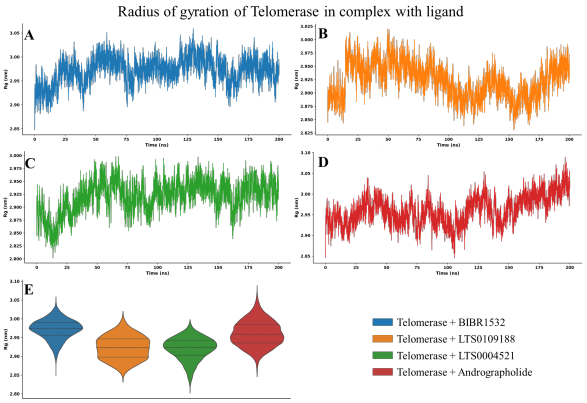

Figure 3: Radius of gyration of telomerase during 200 ns MDS.

*((**A–D**) Telomerase bound to BIBR1532 (blue), LTS0109188 (orange), LTS0004521 (green), or Andrographolide (red). **(E)** Distribution of Rg values summarized by violin plots.)*

Ligand stability during MDS

A critical aspect of MDS is to assess whether ligands remain stably accommodated within the binding pocket rather than drifting away. This was examined by monitoring the RMSD of ligands fitted on the protein backbone, which reflects positional deviation relative to the initial docking pose. As shown in Figure 4A–D, the reference inhibitor BIBR1532 underwent substantial displacement within the first 25 ns, before stabilizing in a new position for the remainder of the 200-ns simulation (Figure 4A). By contrast, LTS0109188 rapidly adapted during the equilibration phase and subsequently maintained a stable binding mode throughout the trajectory (Figure 4B). LTS0004521 exhibited marked fluctuations until 100 ns, after which it achieved a stable configuration for the final 100 ns (Figure 4C). Andrographolide displayed moderate fluctuations within the telomerase pocket without dissociation (Figure 4D). All compounds remained confined within the binding pocket. Importantly, the AP compounds exhibited lower ligand RMSD values compared to BIBR1532, with averages of 0.753 ± 0.062 nm (LTS0109188), 0.635 ± 0.105 nm (LTS0004521), and 0.662 ± 0.118 nm (Andrographolide), versus 0.852 ± 0.165 nm for BIBR1532 (Figure 4E).

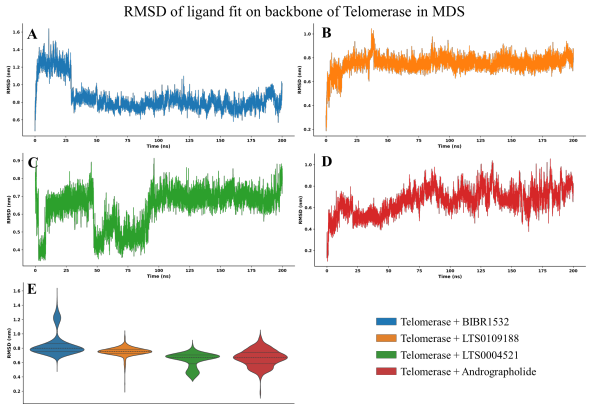

Figure 4: Ligand RMSD relative to the telomerase backbone across MDS.

***((A–D)** Telomerase complexes with BIBR1532 (blue), LTS0109188 (orange), LTS0004521 (green), and Andrographolide (red). **(E)** Comparative RMSD distributions presented as violin plots.)*

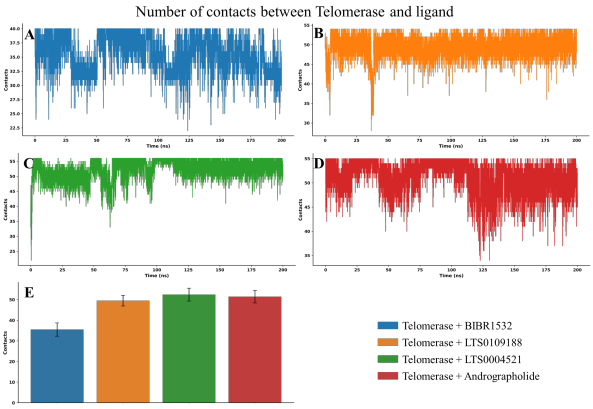

Figure 5: Number of contacts formed between ligands and telomerase during 200 ns MDS.

***((A–D)** Interaction profiles for BIBR1532 (blue), LTS0109188 (orange), LTS0004521 (green), and Andrographolide (red). **(E)** Mean contact numbers per system, summarized as bar plots.)*

Protein–ligand contact analysis

Ligand–protein contacts are a key metric for assessing the strength and persistence of molecular interactions. In the present MDS systems, the number of atomic contacts between telomerase and ligands was quantified and is shown in Figure 5A–D. The reference inhibitor BIBR1532 exhibited relatively unstable interactions, characterized by strong fluctuations throughout the 200-ns simulation (Figure 5A). By contrast, the AP-derived compounds LTS0109188 and LTS0004521 maintained highly stable contact numbers across the trajectory (Figure 5B,C). Andrographolide also exhibited persistent binding, though with moderate fluctuations between 100–200 ns compared to the initial phase of the simulation (Figure 5D). Quantitative analysis revealed that all three AP compounds established significantly higher contact numbers than BIBR1532, with averages of 50 ± 3, 52 ± 3, and 51 ± 3 contacts for LTS0109188, LTS0004521, and Andrographolide, respectively, compared with only 36 ± 3 contacts for BIBR1532. These results indicate stronger and more consistent engagement of the AP compounds with the telomerase binding pocket, thereby underscoring their potential as effective telomerase inhibitors.

Protein–ligand interaction patterns

Characterizing the interaction profiles between ligands and telomerase residues provides critical insights into how compounds are anchored within the binding pocket. Interaction mapping from the MDS trajectories is shown in Figure 6A–D. The reference inhibitor BIBR1532 was stably positioned in a hydrophobic cavity formed by LEU485, VAL491, PHE494, ILE497, and ILE550, and further stabilized by two salt bridges with ARG486 and ARG69 (Figure 6A). LTS0109188 engaged hydrophobic residues PHE494, ILE497, and ILE550, complemented by hydrogen bonding interactions with MET482, ARG486, and GLU549 (Figure 6B). LTS0004521 demonstrated the most extensive binding profile, forming persistent hydrophobic interactions with LEU485, VAL491, PHE494, and TYR551, together with multiple hydrogen bonds involving VAL491, TYR551, LEU554, and GLY553 (Figure 6C). In contrast, Andrographolide was anchored by strong hydrogen bonding to ASN492, a salt bridge with ARG486, and hydrophobic contacts with VAL491, PHE494, ILE497, ILE550, and TYR551 (Figure 6D). Collectively, these analyses highlight ARG486, VAL491, PHE494, ILE497, and ILE550 as key anchoring residues mediating stable ligand binding within the telomerase pocket.

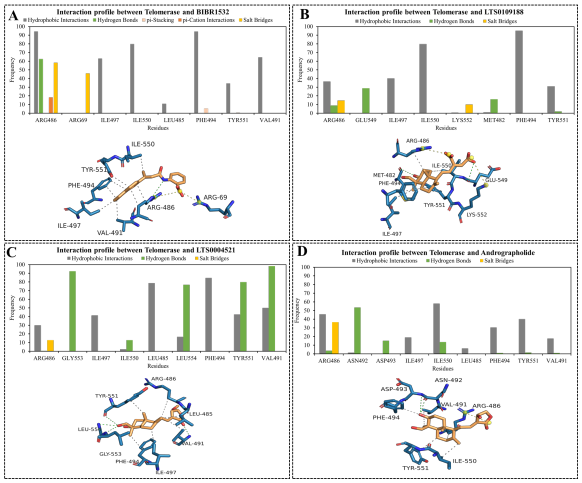

Figure 6: Interaction profiles between telomerase residues and ligands in MDS.

(Stacked bar plots show interaction types: hydrophobic (grey), hydrogen bonds (green), salt bridges (yellow), π–stacking (pink), and π–cation interactions (orange). ***(A)*** *BIBR1532.* ***(B)*** *LTS0109188.* ***(C)*** *LTS0004521.* ***(D)*** *Andrographolide.)*

Binding free energy analysis

Ligand-binding affinity, reflected by binding free energy (BFE), is a crucial parameter for evaluating inhibitory potential toward a target protein[63]. More negative BFE values indicate stronger ligand–protein binding. Among computational approaches, MM/GBSA is widely employed due to its balance of accuracy and computational efficiency in ranking inhibitors[64]. In this study, snapshots from the equilibrated phase of each MDS trajectory (100–200 ns) were used for BFE estimation. Results revealed that BIBR1532 exhibited a mean BFE of –19.090 ± 5.740 kcal/mol. The AP-derived compound LTS0109188 showed a comparable affinity (–20.493 ± 2.209 kcal/mol). Remarkably, LTS0004521 and Andrographolide (LTS0072631) displayed significantly stronger binding, with BFEs of –32.770 ± 2.969 kcal/mol and –23.315 ± 4.078 kcal/mol, respectively. These findings suggest that the AP compounds, particularly LTS0004521 and Andrographolide, bind telomerase more tightly than the reference inhibitor. This reinforces their potential as novel telomerase-directed scaffolds for anticancer drug development.

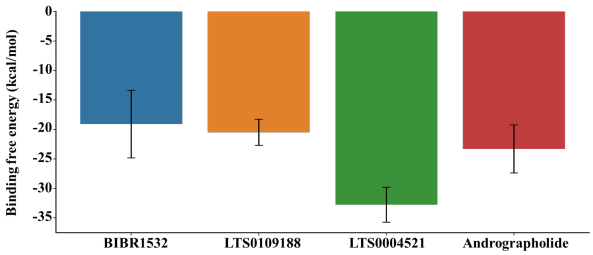

Figure 7: Average binding free energy of ligands bound to telomerase calculated by MM/GBSA.

DISCUSSION

A. paniculata and its bioactive constituents stand out for their tumor-suppressive properties, highlighting their considerable potential in cancer therapy. Inhibition of telomerase activity by 50–80% has been shown to compromise the viability of cancer cells severely[65]. Previous studies have reported that crude extracts of AP suppress telomerase activity, thereby impeding tumor progression[42]. However, the specific compounds within AP responsible for this activity have not been fully elucidated. Phytochemical surveys suggest that, in addition to Andrographolide, its derivatives also contribute significantly to the anticancer activity of AP extracts[66]. This has led to the hypothesis that Andrographolide and its derivatives play a central role in the bioactivity of AP against cancer[67,66]. Moreover, several studies have indicated that Andrographolide may regulate telomerase expression through signaling pathways such as PI3K/AKT/mTOR[68] or NF-κB/MAPK[69]. Nevertheless, direct evidence linking Andrographolide to telomerase inhibition remains inconclusive, underscoring the need for dedicated studies to clarify the molecular mechanism of Andrographolide and its derivatives[43,44].

In this study, molecular docking and dynamic simulations revealed that Andrographolide can stably occupy the catalytic pocket of telomerase. Placement of the compounds at the same anchoring site as BIBR1532 suggests a comparable binding mode. Strikingly, the investigated compounds exhibited stronger binding affinities toward telomerase than BIBR1532. We therefore propose that Andrographolide and its derivatives inhibit telomerase activity via a mechanism analogous to BIBR1532, supported by the conservation of key anchoring residues within the pocket (Figure 6). These findings provide a mechanistic rationale for the development of novel telomerase inhibitors and inform predictions regarding mutations that may alter ligand binding.

Among the compounds, the derivative LTS0004521 demonstrated superior binding compared to Andrographolide (Figure 7). This observation is consistent with prior hypotheses suggesting that the combined action of Andrographolide and its derivatives may converge on telomerase regulation. Expanding these investigations to assess the collective interactions of AP-derived compounds with proteins involved in TERT activation may present a promising avenue toward targeted anticancer therapies with minimal adverse effects.

CONCLUSION

Compounds derived from *A. paniculata*, including Andrographolide and its two derivatives with LOTUS accession numbers LTS0109188 and LTS0004521, were identified to engage telomerase with high affinity, as revealed by molecular docking and dynamic simulations. These compounds exhibited stronger binding compared to the reference inhibitor BIBR1532. Pharmacological profiling, toxicity assessments, and anticancer activity analyses collectively support their potential as safe and orally effective therapeutic candidates. Further exploration of Andrographolide derivatives in AP, alongside experimental validation of these computational findings, will be crucial for advancing their development as telomerase-targeted anticancer agents.

REFERENCES

1. Bray F, Laversanne M, Sung H, Ferlay J, Siegel RL, Soerjomataram I, et al. Global cancer statistics 2022: GLOBOCAN estimates of incidence and mortality worldwide for 36 cancers in 185 countries. CA Cancer J Clin. 2024;74(3):229-63.DOI: 10.3322/caac.21834
2. Artandi SE, DePinho RA. Telomeres and telomerase in cancer. Carcinogenesis. 2010;31(1):9-18.DOI: 10.1093/carcin/bgp268
3. Bajaj S, Kumar MS, Peters GJ, Mayur YC. Targeting telomerase for its advent in cancer therapeutics. Med Res Rev. 2020;40(5):1871-919.DOI: 10.1002/med.21674
4. Fragkiadaki P, Nikitovic D, Kalliantasi K, Sarandi E, Thanasoula M, Stivaktakis PD, et al. Telomere length and telomerase activity in osteoporosis and osteoarthritis. Exp Ther Med. 2020;19(3):1626-32.DOI: 10.3892/etm.2019.8370
5. Vasilopoulos E, Fragkiadaki P, Kalliora C, Fragou D, Docea AO, Vakonaki E, et al. The association of female and male infertility with telomere length (Review). Int J Mol Med. 2019;44(2):375-89.DOI: 10.3892/ijmm.2019.4225
6. Kim NW, Piatyszek MA, Prowse KR, Harley CB, West MD, Ho PL, et al. Specific association of human telomerase activity with immortal cells and cancer. Science. 1994;266(5193):2011-5.DOI: 10.1126/science.7605428
7. Hockemeyer D, Collins K. Control of telomerase action at human telomeres. Nat Struct Mol Biol. 2015;22(11):848-52.DOI: 10.1038/nsmb.3083
8. Sanford SL, Welfer GA, Freudenthal BD, Opresko PL. Mechanisms of telomerase inhibition by oxidized and therapeutic dNTPs. Nat Commun. 2020;11(1):5288.DOI: 10.1038/s41467-020-19115-y
9. Fragkiadaki P, Renieri E, Kalliantasi K, Kouvidi E, Apalaki E, Vakonaki E, et al. Telomerase inhibitors and activators in aging and cancer: A systematic review. Mol Med Rep. 2022;25(5).DOI: 10.3892/mmr.2022.12674
10. Murofushi Y, Nagano S, Kamizono J, Takahashi T, Fujiwara H, Komiya S, et al. Cell cycle-specific changes in hTERT promoter activity in normal and cancerous cells in adenoviral gene therapy: a promising implication of telomerase-dependent targeted cancer gene therapy. Int J Oncol. 2006;29(3):681-8.DOI: 10.3892/ijo.29.3.681
11. Fernández-Varas B, Manguan-García C, Rodriguez-Centeno J, Mendoza-Lupiáñez L, Calatayud J, Perona R, et al. Clinical mutations in the TERT and TERC genes coding for telomerase components induced oxidative stress, DNA damage at telomeres and cell apoptosis besides decreased telomerase activity. Hum Mol Genet. 2024;33(9):818-34.DOI: 10.1093/hmg/ddae015
12. Gillis AJ, Schuller AP, Skordalakes E. Structure of the *Tribolium castaneum* telomerase catalytic subunit TERT. Nature. 2008;455(7213):633-7.DOI: 10.1038/nature07283
13. Jafri MA, Ansari SA, Alqahtani MH, Shay JW. Roles of telomeres and telomerase in cancer, and advances in telomerase-targeted therapies. Genome Med. 2016;8(1):69.DOI: 10.1186/s13073-016-0324-x
14. Picariello L, Grappone C, Polvani S, Galli A. Telomerase activity: an attractive target for cancer therapeutics. World J Pharmacol. 2014;3(4):86-96.DOI: 10.5497/wjp.v3.i4.86
15. Bryan C, Rice C, Hoffman H, Harkisheimer M, Sweeney M, Skordalakes E. Structural Basis of Telomerase Inhibition by the Highly Specific BIBR1532. Structure. 2015;23(10):1934-42.DOI: 10.1016/j.str.2015.08.006
16. Pascolo E, Wenz C, Lingner J, Hauel N, Priepke H, Kauffmann I, et al. Mechanism of human telomerase inhibition by BIBR1532, a synthetic, non-nucleosidic drug candidate. J Biol Chem. 2002;277(18):15566-72.DOI: 10.1074/jbc.M201266200
17. El-Daly H, Kull M, Zimmermann S, Pantic M, Waller CF, Martens UM. Selective cytotoxicity and telomere damage in leukemia cells using the telomerase inhibitor BIBR1532. Blood. 2005;105(4):1742-9.DOI: 10.1182/blood-2003-12-4322
18. Doğan F, Özateş NP, Bağca BG, Abbaszadeh Z, Söğütlü F, Gasımlı R, et al. Investigation of the effect of telomerase inhibitor BIBR1532 on breast cancer and breast cancer stem cells. J Cell Biochem. 2019;120(2):1282-93.DOI: 10.1002/jcb.27089
19. Badrzadeh F, Akbarzadeh A, Zarghami N, Yamchi MR, Zeighamian V, Tabatabae FS, et al. Comparison between effects of free curcumin and curcumin loaded

NIPAAm-MAA nanoparticles on telomerase and PinX1 gene expression in lung cancer cells. Asian Pac J Cancer Prev. 2014;15(20):8931-6.DOI: 10.7314/apjcp.2014.15.20.8931
20. Nasiri M, Zarghami N, Koshki KN, Mollazadeh M, Moghaddam MP, Yamchi MR, et al. Curcumin and silibinin inhibit telomerase expression in T47D human breast cancer cells. Asian Pac J Cancer Prev. 2013;14(6):3449-53.DOI: 10.7314/apjcp.2013.14.6.3449
21. Thai QK, Huynh P, Tran TT, Nguyen BH, Nguyen HTT. Investigating *Andrographis paniculata* Compounds for Apoptosis Induction in Cancer. Asian Pac J Cancer Prev. 2025;26(7):2657-67.DOI: 10.31557/apjcp.2025.26.7.2657
22. Abliz G, Mijit F, Hua L, Abdixkur G, Ablimit T, Amat N, et al. Anti-carcinogenic effects of the phenolic-rich extract from abnormal Savda Munziq in association with its cytotoxicity, apoptosis-inducing properties and telomerase activity in human cervical cancer cells (SiHa). BMC Complement Altern Med. 2015;15:23.DOI: 10.1186/s12906-015-0530-x
23. Jahanban-Esfahlan R, Seidi K, Monfaredan A, Shafie-Irannejad V, Abbasi MM, Karimian A, et al. The herbal medicine Melissa officinalis extract effects on gene expression of p53, Bcl-2, Her2, VEGF-A and hTERT in human lung, breast and prostate cancer cell lines. Gene. 2017;613:14-9.DOI: 10.1016/j.gene.2017.02.034
24. Hossain S, Urbi Z, Karuniawati H, Mohiuddin RB, Moh Qrimida A, Allzrag AM, et al. *Andrographis paniculata* (Burm. f.) Wall. ex Nees: An Updated Review of Phytochemistry, Antimicrobial Pharmacology, and Clinical Safety and Efficacy. Life (Basel). 2021;11(4):348. DOI: 10.3390/life11040348
25. Benoy G, Animesh D, Mandal Aninda MA, Priyanka D, Halder Sandip HS. An overview on *Andrographis paniculata* (Burm. F.) Nees. Int J Res Ayur Pharm. 2012;3(6):752–60.
26. Hossain MS, Urbi Z. Effect of Naphthalene Acetic Acid on the Adventitious Rooting in Shoot Cuttings of *Andrographis paniculata* (Burm.f.) Wall. ex Nees: An Important Therapeutical Herb. Int J Agron. 2016;2016(1):1617543.DOI: 10.1155/2016/1617543
27. Hossain MS, Urbi Z, Sule A, Hafizur Rahman KM. *Andrographis paniculata* (Burm. f.) Wall. ex Nees: a review of ethnobotany, phytochemistry, and pharmacology. Sci World J. 2014;2014:274905.DOI: 10.1155/2014/274905
28. Akbar S. *Andrographis paniculata*: a review of pharmacological activities and clinical effects. Altern Med Rev. 2011;16(1):66-77.
29. Jarukamjorn K, Nemoto N. Pharmacological aspects of *Andrographis paniculata* on health and its major diterpenoid constituent andrographolide. J Health Sci. 2008;54(4):370-81.DOI: 10.1248/jhs.54.370
30. Kumar RA, Sridevi K, Kumar NV, Nanduri S, Rajagopal S. Anticancer and immunostimulatory compounds from *Andrographis paniculata*. J Ethnopharmacol. 2004;92(2-3):291-5.DOI: 10.1016/j.jep.2004.03.004
31. Matsuda T, Kuroyanagi M, Sugiyama S, Umehara K, Ueno A, Nishi K. Cell differentiation-inducing diterpenes from *Andrographis paniculata* Nees. Chem Pharm Bull (Tokyo). 1994;42(6):1216-25.DOI: 10.1248/cpb.42.1216
32. Li W, Xu X, Zhang H, Ma C, Fong H, van Breemen R, et al. Secondary metabolites from *Andrographis paniculata*. Chem Pharm Bull (Tokyo). 2007;55(3):455-8.DOI: 10.1248/cpb.55.455
33. Cheung HY, Cheung SH, Li J, Cheung CS, Lai WP, Fong WF, et al. Andrographolide isolated from Andrographis paniculata induces cell cycle arrest and mitochondrial-mediated apoptosis in human leukemic HL-60 cells. Planta Med. 2005;71(12):1106-11.DOI: 10.1055/s-2005-873128
34. Paul S, Roy D, Pati S, Sa G. The Adroitness of Andrographolide as a Natural Weapon Against Colorectal Cancer. Front Pharmacol. 2021;12:731492.DOI: 10.3389/fphar.2021.731492
35. Kumar S, Singh B, Bajpai V. *Andrographis paniculata* (Burm.f.) Nees: Traditional uses, phytochemistry, pharmacological properties and quality control/quality assurance. J Ethnopharmacol. 2021;275:114054.DOI: 10.1016/j.jep.2021.114054
36. Chakravarti RN, Chakravarti D. Andrographolide, the active constituent of *Andrographis paniculata Nees*; a preliminary communication. Ind Med Gaz. 1951;86(3):96-7.
37. Rajagopal S, Kumar RA, Deevi DS, Satyanarayana C, Rajagopalan R. Andrographolide, a potential cancer therapeutic agent isolated from *Andrographis paniculata*. J Exp Ther Oncol. 2003;3(3):147-58.DOI: 10.1046/j.1359-4117.2003.01090.x
38. Adiguna SP, Panggabean JA, Atikana A, Untari F, Izzati F, Bayu A, et al. Antiviral Activities of Andrographolide and Its Derivatives: Mechanism of Action and Delivery System. Pharmaceuticals (Basel). 2021;14(11): 1102.DOI: 10.3390/ph14111102
39. Yadav RP, Sadhukhan S, Saha ML, Ghosh S, Das M. Exploring the mechanism of andrographolide in the treatment of gastric cancer through network pharmacology and molecular docking. Sci Rep. 2022;12(1):18413.DOI: 10.1038/s41598-022-18319-0

40. Peng Y, Wang Y, Tang N, Sun D, Lan Y, Yu Z, et al. Andrographolide inhibits breast cancer through suppressing COX-2 expression and angiogenesis via inactivation of p300 signaling and VEGF pathway. J Exp Clin Cancer Res. 2018;37(1):248.DOI: 10.1186/s13046-018-0926-9
41. Chen W, Feng L, Nie H, Zheng X. Andrographolide induces autophagic cell death in human liver cancer cells through cyclophilin D-mediated mitochondrial permeability transition pore. Carcinogenesis. 2012;33(11):2190-8.DOI: 10.1093/carcin/bgs264
42. Budiatin AS, Sagitaras IB, Nurhayati IP, Khairah N, Nisak K, Susilo I, et al. Attenuation of hyperplasia in lung parenchymal and colonic epithelial cells in DMBA-induced cancer by administering *Andrographis paniculata* Nees extract using animal model. J Basic Clin Physiol Pharmacol. 2021;32(4):497-504.DOI: 10.1515/jbcpp-2020-0440
43. Valdiani A, Ofoghi H, Akbarizare M, Talei D. *Andrographis paniculata* extract as an immunity modulator against cancer via telomerase inhibition. 3 Biotech. 2022;12(11):319.DOI: 10.1007/s13205-022-03373-2
44. Hu J, Li Y, Xie X, Song Y, Yan W, Luo Y, et al. The therapeutic potential of andrographolide in cancer treatment. Biomed Pharmacother. 2024;180:117438.DOI: 10.1016/j.biopha.2024.117438
45. O'Boyle NM, Banck M, James CA, Morley C, Vandermeersch T, Hutchison GR. Open Babel: An open chemical toolbox. J Cheminform. 2011;3(1):33.DOI: 10.1186/1758-2946-3-33
46. Morris GM, Huey R, Lindstrom W, Sanner MF, Belew RK, Goodsell DS, et al. AutoDock4 and AutoDockTools4: Automated docking with selective receptor flexibility. J Comput Chem. 2009;30(16):2785-91.DOI: 10.1002/jcc.21256
47. Santos-Martins D, Solis-Vasquez L, Tillack AF, Sanner MF, Koch A, Forli S. Accelerating AutoDock4 with GPUs and Gradient-Based Local Search. J Chem Theory Comput. 2021;17(2):1060-73.DOI: 10.1021/acs.jctc.0c01006
48. Adasme MF, Linnemann KL, Bolz SN, Kaiser F, Salentin S, Haupt V J, et al. PLIP 2021: expanding the scope of the protein–ligand interaction profiler to DNA and RNA. Nucleic Acids Res. 2021;49(W1):W530-W4.DOI: 10.1093/nar/gkab294
49. Daina A, Michielin O, Zoete V. SwissADME: a free web tool to evaluate pharmacokinetics, drug-likeness and medicinal chemistry friendliness of small molecules. Sci Rep. 2017;7(1):42717.DOI: 10.1038/srep42717
50. Pires DE, Blundell TL, Ascher DB. pkCSM: Predicting Small-Molecule Pharmacokinetic and Toxicity Properties Using Graph-Based Signatures. J Med Chem. 2015;58(9):4066-72.DOI: 10.1021/acs.jmedchem.5b00104
51. Lagunin A, Stepanchikova A, Filimonov D, Poroikov V. PASS: prediction of activity spectra for biologically active substances. Bioinformatics. 2000;16(8):747-8.DOI: 10.1093/bioinformatics/16.8.747
52. Zoete V, Cuendet MA, Grosdidier A, Michielin O. SwissParam: a fast force field generation tool for small organic molecules. J Comput Chem. 2011;32(11):2359-68.DOI: 10.1002/jcc.21816
53. Abraham MJ, Murtola T, Schulz R, Páll S, Smith JC, Hess B, et al. GROMACS: High performance molecular simulations through multi-level parallelism from laptops to supercomputers. SoftwareX. 2015;1:19-25.DOI: 10.1016/j.softx.2015.06.001
54. Huang J, MacKerell AD, Jr. CHARMM36 all-atom additive protein force field: validation based on comparison to NMR data. J Comput Chem. 2013;34(25):2135-45.DOI: 10.1002/jcc.23354
55. Khan A, Chandra Kaushik A, Ali SS, Ahmad N, Wei DQ. Deep-learning-based target screening and similarity search for the predicted inhibitors of the pathways in Parkinson's disease. RSC Adv. 2019;9(18):10326-39.DOI: 10.1039/c9ra01007f
56. Ali A, Khan MT, Khan A, Ali S, Chinnasamy S, Akhtar K, et al. Pyrazinamide resistance of novel mutations in pncA and their dynamic behavior. RSC Adv. 2020;10(58):35565-73.DOI: 10.1039/d0ra06072k
57. Khan A, Waris H, Rafique M, Suleman M, Mohammad A, Ali SS, et al. The Omicron (B.1.1.529) variant of SARS-CoV-2 binds to the hACE2 receptor more strongly and escapes the antibody response: Insights from structural and simulation data. Int J Biol Macromol. 2022;200:438-48.DOI: 10.1016/j.ijbiomac.2022.01.059
58. Valdés-Tresanco MS, Valdés-Tresanco ME, Valiente PA, Moreno E. gmx_MMPBSA: A New Tool to Perform End-State Free Energy Calculations with GROMACS. J Chem Theory Comput. 2021;17(10):6281-91.DOI: 10.1021/acs.jctc.1c00645
59. Kufareva I, Abagyan R. Methods of protein structure comparison. Methods Mol Biol. 2012;857:231-57.DOI: 10.1007/978-1-61779-588-6_10
60. De Vita S, Chini MG, Bifulco G, Lauro G. Insights into the Ligand Binding to Bromodomain-Containing Protein 9 (BRD9): A Guide to the Selection of Potential Binders by Computational Methods. Molecules. 2021;26(23):7192.DOI: 10.3390/molecules26237192

61. Newcomer ME, Lewis BA, Quiocho FA. The radius of gyration of L-arabinose-binding protein decreases upon binding of ligand. J Biol Chem. 1981;256(24):13218-22.
62. Olah GA, Trakhanov S, Trewhella J, Quiocho FA. Leucine/isoleucine/valine-binding protein contracts upon binding of ligand. J Biol Chem. 1993;268(22):16241-7.
63. Genheden S, Ryde U. The MM/PBSA and MM/GBSA methods to estimate ligand-binding affinities. Expert Opin Drug Discov. 2015;10(5):449-61.DOI: 10.1517/17460441.2015.1032936
64. Hou T, Wang J, Li Y, Wang W. Assessing the performance of the MM/PBSA and MM/GBSA methods. 1. The accuracy of binding free energy calculations based on molecular dynamics simulations. J Chem Inf Model. 2011;51(1):69-82.DOI: 10.1021/ci100275a
65. Shay JW, Wright WE. Mechanism-based combination telomerase inhibition therapy. Cancer Cell. 2005;7(1):1-2.DOI: 10.1016/j.ccr.2004.12.012
66. Suriyo T, Pholphana N, Rangkadilok N, Thiantanawat A, Watcharasit P, Satayavivad J. *Andrographis paniculata* extracts and major constituent diterpenoids inhibit growth of intrahepatic cholangiocarcinoma cells by inducing cell cycle arrest and apoptosis. Planta Med. 2014;80(7):533-43.DOI: 10.1055/s-0034-1368399
67. Geethangili M, Rao YK, Fang SH, Tzeng YM. Cytotoxic constituents from Andrographis paniculata induce cell cycle arrest in jurkat cells. Phytother Res. 2008;22(10):1336-41.DOI: 10.1002/ptr.2493
68. Duan MX, Zhou H, Wu QQ, Liu C, Xiao Y, Deng W, et al. Andrographolide Protects against HG-Induced Inflammation, Apoptosis, Migration, and Impairment of Angiogenesis via PI3K/AKT-eNOS Signalling in HUVECs. Mediators Inflamm. 2019;2019:6168340.DOI: 10.1155/2019/6168340
69. Li Y, He S, Tang J, Ding N, Chu X, Cheng L, et al. Andrographolide Inhibits Inflammatory Cytokines Secretion in LPS-Stimulated RAW264.7 Cells through Suppression of NF-κB/MAPK Signaling Pathway. Evid Based Complement Alternat Med. 2017;2017:8248142.DOI: 10.1155/2017/8248142